Journal of Alloys and Compounds 501 (2010) 18–24

Contents lists available at ScienceDirect

Journal of Alloys and Compounds

journal homepage: www.elsevier.com/locate/jallcom

Phase formation during mechanically activated annealing of nanocrystalline Cr–60at.%Al

M.S. Archana, Neha Hebalkar, K. Radha, J. Joardar*

Centre for Nanomaterials, International Advanced Research Centre for Powder Metallurgy and New Materials (ARCI), PO Balapur, Hyderabad 500005, India

ARTICLE INFO

Article history:
Received 22 January 2010
Received in revised form 2 April 2010
Accepted 7 April 2010
Available online 14 April 2010

Keywords:
Peritectic
Phase transformation
Cr_5Al_8
Nanocrystalline
Mechanical alloying

ABSTRACT

Evolution of phases during mechanically activated annealing (MA2) of nanocrystalline Cr–Al powder blend with peritectic $Cr_{40}Al_{60}$ composition was investigated. Significant interdiffusion was observed during MA2 at a low temperature of 400 °C, which led to the formation of various Cr–Al phases viz. tetragonal (*I4/mmm*) Cr_2Al, rhombohedral (*R3m*) $Cr_{9.5}Al_{16}$ and the high temperature cubic (*I-43m*) β-Cr_5Al_8. Such diffusion-induced phase formation was observed only at a higher temperature of 850 °C in case of a coarse (~50 μm) grade Cr–60at.%Al precursor. Hexagonal ($P6_3/mmc$) Cr_2AlC phase was also obtained on annealing of the ball-milled nanocrystalline precursor. The carbide phase formation was attributed to the presence of milling-induced C-contamination (~2.65–2.80 wt.%) in the ball-milled precursor. The Cr_2AlC phase apparently evolved from Cr_2Al in the temperature range of 400–850 °C.

1. Introduction

Mechanically activated annealing (MA2) [1–14] has drawn wide interest in the synthesis of various alloys and compounds. The process involves heating of the mechanically deformed or high energy ball-milled powder blends at a temperature much below the equilibrium phase formation temperature. MA2 has been beneficial in several systems, which are otherwise difficult to synthesize by mechanical alloying (MA). Usually, these 'difficult-to-synthesize' phases belong to immiscible or slow-diffusing systems, where the phase formation is difficult, if not impossible, even at nanocrystalline state. The evolution of peritectic intermetallic phases by MA or MA2 is noteworthy in this regard as these are observed in slow-diffusing systems. As per the equilibrium phase diagram, a peritectic reaction involves a liquid phase in the invariant reaction $L + \beta \rightarrow \alpha$. Since MA and MA2 are low temperature solid-state processing, equilibrium peritectic reaction involving liquid phase is not expected. Therefore, its evolution may be termed as peritectic transformation wherein the peritectic α-phase may form by long-range diffusion [15].

In spite of the fact that several technologically important peritectic compounds are known to exist and some of which have been synthesized by MA or MA2, the underlying phase formation mechanism is not well established. A list of peritectic aluminides synthesized by mechanically activated processing is presented in Table 1. Apart from the peritectic aluminides, various other compounds, e.g., borides [12] and composites [13,14] have been reported by MA2. The list of the phases and the accompanying data in Table 1 apparently indicate that the formation of peritectic aluminides by MA or MA2 is not determined by the equilibrium reaction temperature or the enthalpy of formation.

Peritectic phases in Cr–Al system present a unique situation, where the enthalpy of the phase formation is less negative (ref. Table 1) and Cr has low diffusivity in Al. Studies on the synthesis of peritectic phases in Cr–Al system by MA or MA2 are limited. In a recent work, high temperature Cr_5Al_8 phase formation was observed at intermediate stages during low temperature (420 °C) annealing of a mechanically milled Cr-rich $Cr_{65}Al_{35}$ blend, which corresponds to the Cr_2Al phase field [16].

Equilibrium Cr–Al phase diagram has been studied extensively by several groups [34–39]. The binary Cr–Al system consists of six intermediate phases viz. Cr_5Al_8, Cr_4Al_9, $CrAl_4$, Cr_2Al_{11}, $CrAl_7$ and Cr_2Al (Fig. 1), five of which evolve via peritectic reaction [38,39]. Apart from academic interest, the Cr–Al alloys find application in various fields. For example, Al-based alloys with high concentration of slow-diffusing Cr along with other metals like Fe, Zr, etc., are employed in high-temperature applications and aerospace industries due to their thermal stability and low specific weight [40]. Cr–Al alloy thin films have high resistivity and good heat-resistance which makes them a suitable candidate for highly integrated electronic components [41].

In this paper, we have discussed the formation and stability of peritectic Cr_5Al_8 and other Cr–Al phases during MA2 of nanocrystalline powder blend with peritectic $Cr_{40}Al_{60}$ composition. The

* Corresponding author. Tel.: +91 40 24441076; fax: +91 40 24442699.
E-mail addresses: joydip@arci.res.in, joydip@lycos.com (J. Joardar).

0925-8388/$ – see front matter © 2010 Elsevier B.V. All rights reserved.
doi:10.1016/j.jallcom.2010.04.046

Table 1
Peritectic phases in aluminides by mechanically activated process.

System A–B	Phase	Space group	Invariant reaction	Reaction temperature (°C)	ΔH_f^{298K} (kJ/mol)	Method	Ref
Al–Cr	Al_7Cr	*C2/m*	L+$Al_{11}Cr_2$	790	−13.4	NR	
	$Al_{11}Cr_2$	*P2*	L+Al_4Cr	940	−15.0	NR	
	Al_4Cr	*P2/m*	L+Al_8Cr_5	1030	−17.0	NR	
	Al_8Cr_5	*I-43m*	L+(Cr)	1350	−15.0	MA+HT (420)	[16]
Al–Ti	AlTi	*P4/mmm*	L+α-Ti	1460	−40.1	MA+HT (635)	[17,18]
	$Al_{11}Ti_5$	*I4/mmm*	L+$Al_{1+x}Ti_{1-x}$	1416	−40.2	NR	
	Al_3Ti	*I4/mmm*	L+$Al_{11}Ti_5$	1387	−36.6	MA, MA+HT (300, 1000)	[19–21]
Al–Ni	$AlNi_3$	*P4/mmm*	L+AlNi	1395	−40.1	MA, MA+HT (350, 950)	[22–24]
	Al_3Ni_2	*P-3m1*	L+AlNi	1133	−57.6	MA, MA+HT (477)	[25–27]
	Al_3Ni	*Pnma*	L+Al_3Ni_2	854	−37.7	MA, MA+HT (400)	[28,29]
Al–Fe	Al_8Fe_5	*I4-3m*	L+AlFe	1215	−25.0	NR	
Al–Mo	Al_4Mo	*Cm*	L+Al_8Mo_3	1130	−37.0	MA+HT (697)[a]	[30]
	Al_5Mo	*R-3c*	L+Al_4Mo	735	−32.0	MA+HT (670)	[30,31]
	$Al_{12}Mo$	*Im-3*	L+Al_5Mo	700	−15.0	MA+HT (397)	[30,31]
Al–Nb	Nb3Al	*Pm3-n*	L+(Nb)	2060	−13.7	MM+HT (800)	[32]
Al–Ru	Ru_2Al_5	*Cmcm*	L+$RuAl_2$	1492	−44.7	MA+HT (550)	[33]

MA = mechanical alloying; HT (****) = heat treatment (temperature, °C); NR = not reported.
[a] Trace amount.

polymorphic transition between the low temperature rhombohedral (*R3m*) and high temperature cubic (*I-43m*) Cr_5Al_8 under MA2 was also investigated.

2. Experimental

Chromium (CERAC™; 99.5%purity; −325 mesh size) and aluminium (Alfa-Aesar™; 99.5% purity; −325 mesh size) powders were blended with a composition of Cr–60at.%Al by high-energy ball-milling in a planetary ball mill (Pulverisette P5, Fritsch GmbH). The milling was done for 20 h at 250 rpm in a cemented carbide vial under toluene bath at a ball-to-powder weight ratio (BPR) of 15:1. For a comparative study, Cr and Al powders in identical proportion were blended in a low-energy horizontal pot mill for 20 h under toluene bath at a BPR of 5:1. After milling or blending the powders were dried before loading in the furnace for annealing. Small amount of the powder samples were taken in alumina boat and annealed under vacuum (10^{-3} Torr) in a horizontal tube furnace. The annealing was done at 400, 500, 600 and 850 °C. The heating rate of 5 °C/min and holding period of 2 h was maintained for all annealing experiments unless stated otherwise. The samples were subsequently furnace cooled to room temperature under vacuum.

The phase evolution in the powder samples at various stages was monitored by X-ray diffraction (XRD) using BRUKER D8 Max Advance system. Cu Kα radiation in step scan mode was employed for this purpose. The quantitative analysis of the XRD profiles was done using FullProf version 4.0 Rietveld structural refinement software [42]. The microstructure of the powder samples was investigated by transmission electron microscopy (TEM) using Tecnai G^2 (200 kV) system. The samples for TEM analysis were prepared by first dispersing the powder in ethanol by ultrasonication and subsequently high pressure homogenization of the dispersion using homogenizer (EmulsiFlex C5, Avestin Inc.). The carbon content in the samples was estimated using carbon analyzer (LECO CS 400).

3. Results and discussion

Fig. 2a shows the XRD profile of the mechanically milled (MM) powder blend and also the profiles after its heat treatment at various temperatures. The profile for the unmilled powder is also shown for comparison. Significant broadening of the XRD peaks was observed for the MM powder when compared with the unmilled blend, indicating the nanocrystalline nature of the MM powder. However, no new phase formation was detected during MM for 20 h as evident from the XRD phase analysis. The crystallite sizes

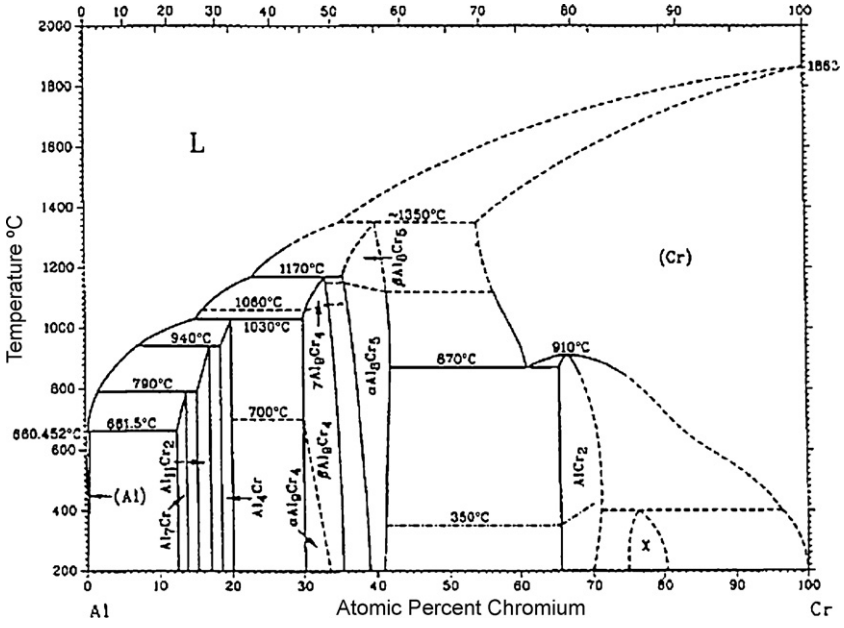

Fig. 1. Phase diagram of Cr–Al [38].

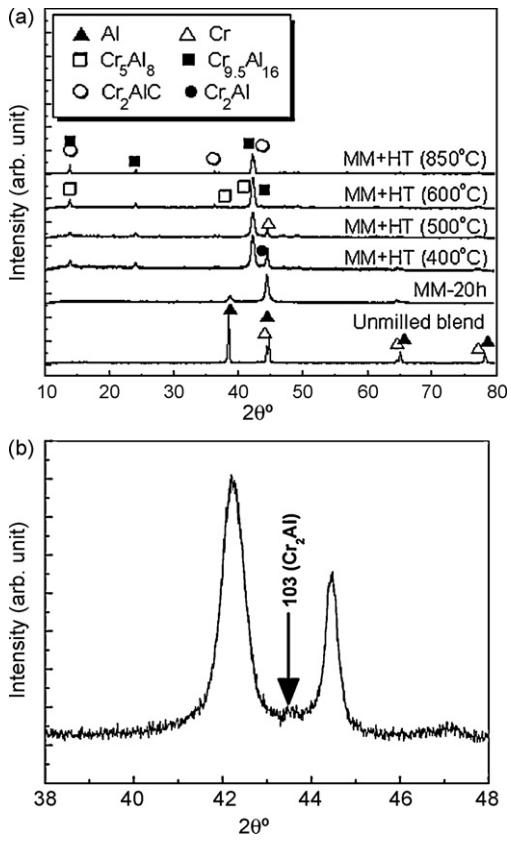

Fig. 2. (a) XRD patterns of MM and MA2 samples at temperatures 400, 500, 600 and 850 °C. (b) Magnified section of the profile for MM + HT 400 °C showing 103 peak of Cr_2Al.

of Al and Cr in the MM powder blend, as estimated from the peak broadening by Scherrer's formula [43], were about 14 and 18 nm, respectively. The TEM studies (Fig. 3), on the other hand, indicate that the ball-milled Cr–Al powder blends are nanostructured with an average particle size in the range of 5–8 nm. The higher crystallite size data from XRD could be due to the fact that XRD provides information on the average size while TEM takes into account only the finer particles, which remains suspended in the organic solvent during sample preparation. The XRD profiles in Fig. 2 further illustrate that the peak due to free nanocrystalline Al in the mechanically milled precursor (MM for 20 h), disappears on heating at 400 °C, while the nanocrystalline Cr-peaks are retained even at 600 °C. A careful phase analysis of the XRD profiles reveals multiple Cr–Al phase formation on annealing of the MM powder blend at 400 °C. The observed phases include tetragonal (*I4/mmm*) Cr_2Al, low temperature rhombohedral (*R3m*) $Cr_{9.5}Al_{16}$ and also the high temperature cubic (*I-43m*) β-Cr_5Al_8. A magnified section of the profile for the MM powder heat treated at 400 °C is shown in Fig. 2b, in order to illustrate the presence of small fraction of Cr_2Al. The presence of the phase was validated by the minimization of the agreement factors viz. weighted profile factor R_{wp} and the goodness-of-fit index (GoF) during Rietveld refinement. The agreement factor, R_{wp}, is given by $R_{wp} = 100[\sum_{i=1,n} w_i|y_i - y_{c,i}|^2/\sum_{i=1,n} w_i y_i^2]^{1/2}$ and GoF = R_{wp}/R_{exp}, where $w_i = 1/\sigma_i^2$, σ_i^2 being the variance of the observation y_i while R_{exp} is the expected weighted profile factor given by $R_{exp} = 100[(n-p)/\sum_i w_i y_i^2]^{1/2}$ for '*n*' number of points used in the refinement with '*p*' number of refined parameters.

The Cr-peak intensity in Fig. 2a gradually diminishes with the increase in the annealing temperature. This possibly indicates a drop in free Cr, apparently due to its diffusion into various intermetallic phases formed at lower temperature. At higher annealing temperature of 850 °C, the low temperature $Cr_{9.5}Al_{16}$ is the only binary phase in the system apart from Cr_2AlC.

Low intensity peaks of Cr_2AlC phase was detected in the MA2 samples at 400 °C, which is substantially lower than that reported previously (850 °C) for coarse grade precursor [44]. It may be noted that Cr_2AlC, which is a $M_{n+1}AX_n$ or MAX system (where M is early transition metal, A is a IIIA or IVA element, X is C or N and $n = 1, 2, 3$), has excellent high temperature oxidation resistance along with high elastic modulus and high room temperature plasticity [45,46]. The solubility of C in Al is negligible even at higher temperature of 1300–1500 °C, while it is about 0.0535 at.% at the eutectic temperature (1490 °C) in Cr [47]. Consequently, the formation of Cr or Al-based carbides are not expected at low temperature. It is plausible that the formation of Cr–Al compounds like Cr_2Al facilitated the Cr_2AlC formation by diffusion of C into the aluminide as proposed earlier [44]. Carbon analyses of the ball-milled as well as the MA2 processed samples showed nearly 2.65–2.80 wt.% of carbon in the system. Such high carbon pick up during high-energy mechanical milling is possible due to degradation of the toluene, which was added as a process control agent (PCA).

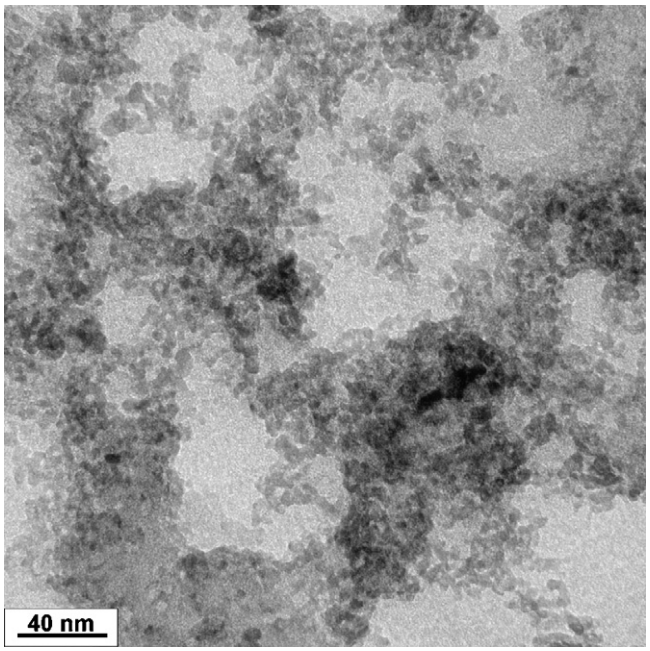

Fig. 3. TEM micrograph of mechanically milled Cr–Al powder showing nanostructured particles.

The weight fraction and lattice parameter data for the phases evolved during MA2 were estimated by Rietveld structural refinement of the XRD profiles. The lattice parameter data for the various phases, agreement factors viz. R_{wp} and GoF index values for the Rietveld refinement are presented in Table 2. Fig. 4a shows a typical Rietveld refined profile for a powder sample after MA2 at 850 °C indicating the presence of two phases viz. $Cr_{9.5}Al_{16}$ and Cr_2AlC. The highly overlapped maximum intensity peak is decomposed in Fig. 4b for clarity. It is evident from the data in Table 2 and Fig. 5 that β-Cr_5Al_8 fraction increases till 600 °C and is, however, absent at higher temperature of 850 °C while Cr_2Al and Cr phase fraction decreases till 600 °C and disappears at 850 °C. Cr_2AlC phase, on-the-other-hand, shows a gradual rise with temperature and seems to have reached a saturation level at or beyond 600 °C. The results indicate that the depletion of Cr_2Al and Cr is followed by increase in the Cr_2AlC fraction, which apparently points to preferential carburization of Cr_2Al over $Cr_{9.5}Al_{16}$ and β-Cr_5Al_8 phases. The Cr_2AlC

Table 2
Rietveld refined data on lattice parameters of the phases obtained by MA2 of nanocrystalline Cr–60at.%Al.

Temperature (°C)	Dwell time (h)	Phases	Lattice parameter (Å)			R_{wp} (GoF)
			a	*b*	*c*	
400	2	Cr	2.88207	2.88207	2.88207	6.99 (1.1)
		Cr_2Al	3.00984	3.00984	8.62080	
		Cr_2AlC	2.85935	2.85935	12.80978	
		Cr_5Al_8	9.08415	9.08415	9.08415	
		$Cr_{9.5}Al_{16}$	12.74556	12.74556	7.95007	
500	2	Cr	2.88307	2.88307	2.88307	6.80 (1.2)
		Cr_2Al	3.01220	3.01220	8.60568	
		Cr_2AlC	2.85570	2.85570	12.81175	
		Cr_5Al_8	9.08414	9.08414	9.08414	
		$Cr_{9.5}Al_{16}$	12.73395	12.73395	7.95490	
600	2	Cr	2.88392	2.88392	2.88392	7.33 (1.2)
		Cr_2Al	3.00984	3.00984	8.62080	
		Cr_2AlC	2.85935	2.85935	12.80978	
		Cr_5Al_8	9.07912	9.07912	9.07912	
		$Cr_{9.5}Al_{16}$	12.75121	12.75121	7.94829	
850	0	Cr_2AlC	2.86160	2.86160	12.81710	7.57 (1.3)
		$Cr_{9.5}Al_{16}$	12.76610	12.76610	7.95020	
	2	Cr_2AlC	2.86009	2.86009	12.80919	7.93 (1.3)
		$Cr_{9.5}Al_{16}$	12.75540	12.75540	7.94560	

phase possibly forms by one of the reactions proposed earlier for coarse grade Cr–Al [44] viz. $Cr_2Al + C \rightarrow Cr_2AlC$. The $Cr_{9.5}Al_{16}$ phase shows a sharp rise only above 600 °C, which implies that the rhombohedral (*R3m*) $Cr_{9.5}Al_{16}$ phase is thermodynamically more stable when compared to the high temperature cubic β-Cr_5Al_8 in the temperature range of 600–850 °C.

It is worthwhile mentioning that the preferential carburization of Cr_2Al over other phases may be due to the presence of consecutive Cr–Cr planes with octahedral voids in the tetragonal (*I4/mmm*) structure. The atomic arrangement in Cr_2Al and Cr_2AlC are shown in Fig. 6. The calculated octahedral void size in Cr_2Al is 0.864 Å. Consequently, the carbon atom, which has a covalent radius of 0.76 Å [48], is expected to enter Cr_2Al lattice only under thermodynamically favorable conditions. It may be noted that the (1 0 0) and ($\bar{1}$ 0 0) planes of Cr_2Al shown in (Fig. 6a) has interplanar spacing of 1.917 Å. After carburization, the (1 0 0) and ($\bar{1}$ 0 0) spacing increases by 0.4337 Å (to 2.354 Å) to accommodate the C atom in the lattice (Fig. 6b). The absence of consecutive Cr–Cr planes and sufficient void space in the lattice structure of Cr_5Al_8 and $Cr_{9.5}Al_{16}$ do not favor diffusion of C in the lattice.

Fig. 7 shows the high resolution TEM micrograph of MA2 sample at 600 °C. The different interplanar spacing in the micrograph indicates the presence of multiple phases as also confirmed by XRD. However, the phase composition for the individual grains could not be ascertained due to similar lattice spacing in different phases present in the system. The crystallite sizes appeared to be in the range of 5–15 nm. The TEM micrographs of the samples subjected to MA2 at 850 °C (Fig. 8a and b), on-the-other-hand, show interplanar spacing of 0.25 and 0.29 nm, which corresponds to (1 0 0) of Cr_2AlC and (1 2 2) of $Cr_{9.5}Al_{16}$, respectively. The $Cr_{9.5}Al_{16}$ grains were nanostructured (~15 nm) while it was difficult to ascertain the grain size of Cr_2AlC from the TEM micrographs as the particles appeared to be in a highly agglomerated state.

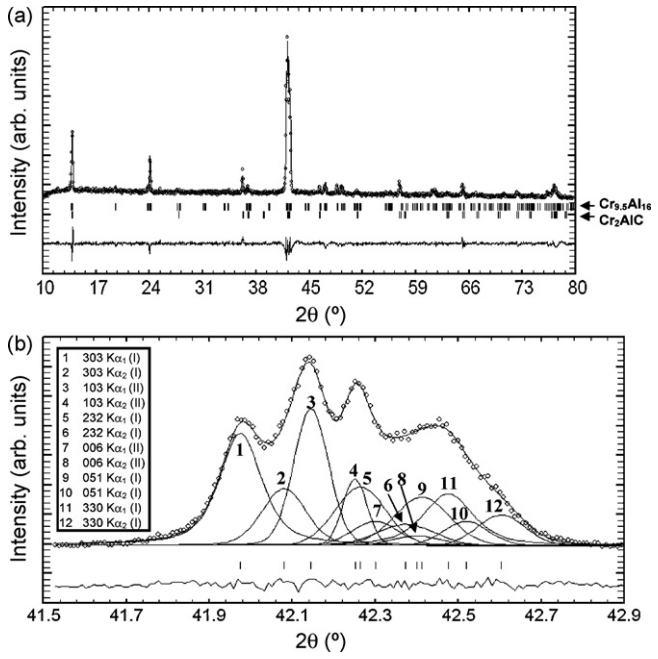

Fig. 4. (a) Rietveld refined XRD profile of MA2 sample at 850 °C showing $Cr_{9.5}Al_{16}$ and Cr_2AlC phases. (b) Decomposed maximum intensity peak of the XRD profile for MA2 at 850 °C indicating $Cr_{9.5}Al_{16}$(I) and Cr_2AlC(II).

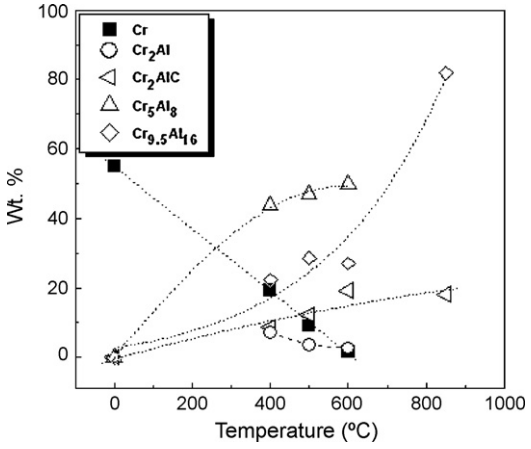

Fig. 5. Change in the fraction of various phases with annealing temperature.

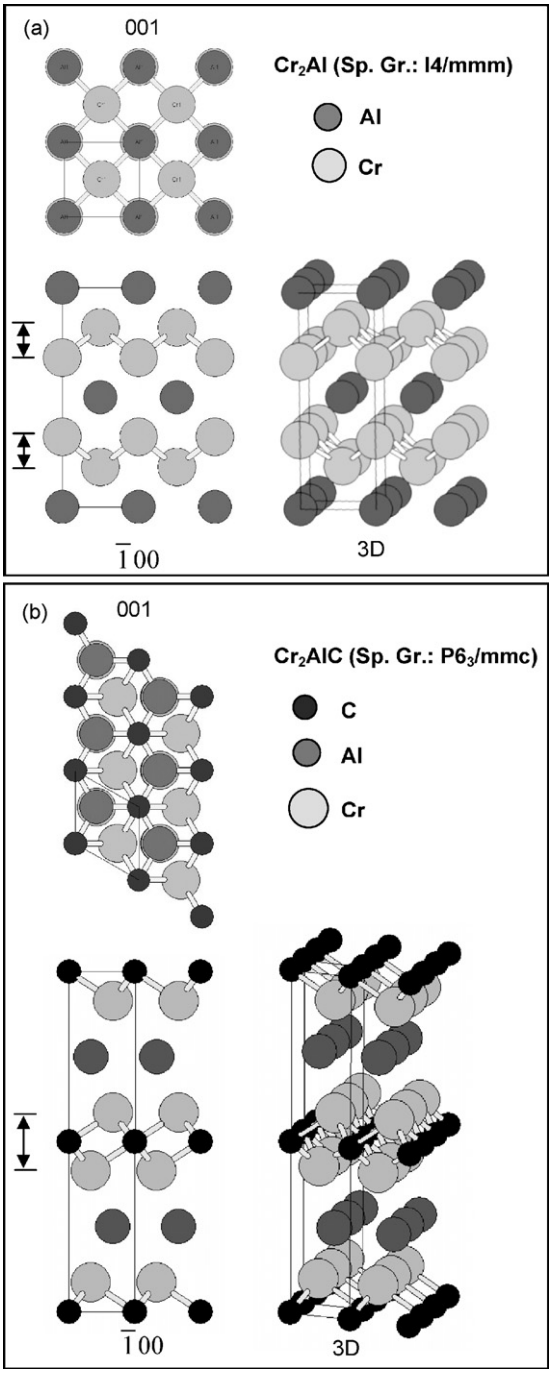

Fig. 6. Atomic arrangement in 0 0 1 and $\bar{1}$ 0 0 view along with 3D representation of (a) Cr_2Al and (b) Cr_2AlC.

The variation of the lattice parameter of Cr after ball milling and subsequent annealing is shown in Fig. 9. It is evident that there is an increase in the lattice parameter of Cr even after ball-milling. However, the lattice parameter drops on annealing at 400 °C but shows marginal increase with increase in annealing temperature. The initial shift in the lattice parameter on ball-milling may be due to the dissolution of Al in nanocrystalline Cr as well as the lattice strain caused by severe deformation during mechanical activation. Subsequent drop in the lattice parameter could be attributed to the removal of lattice strain at elevated temperature. The increase in lattice parameter with annealing temperature possibly reflects the dissolution of Al and/or C in nanocrystalline Cr. However, this could not be confirmed from the TEM studies.

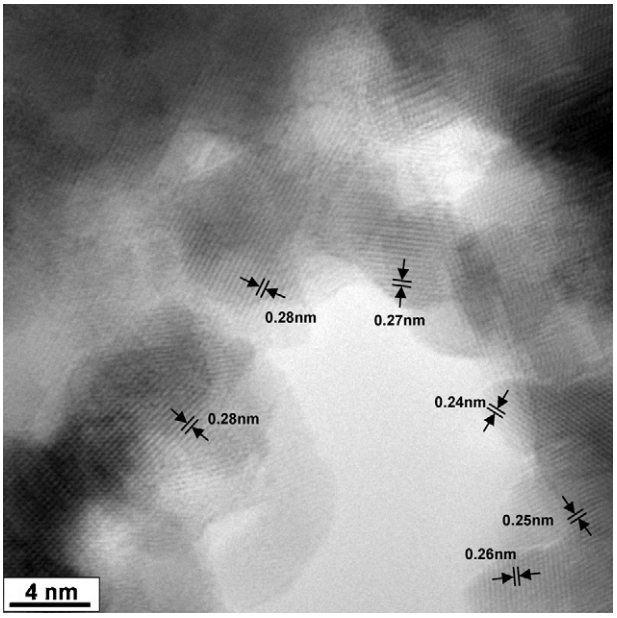

Fig. 7. High resolution TEM micrograph of MA2 sample at 600 °C.

In order to evaluate the influence of milling-induced nanocrystalline Cr–Al structure on the MA2 process, a comparative study was done with identical composition comprising of coarse (50 μm) grade powder blend prepared by low-energy conventional horizontal blender (pot mill). Fig. 10a shows the XRD profile of the blend and the profiles after subsequent annealing at temperatures in the range of 400–850 °C. Insignificant broadening of the Cr and Al peaks in the XRD profile was observed for the blend obtained after pot milling for 20 h indicating the coarse crystallite size of the powder. It is evident from Fig. 10 that Cr and Al apparently remains in a free-state even at 600 °C with no trace of any other phase. At higher temperature of 850 °C, on-the-other-hand, Cr_2Al, Cr_7Al_{45}, $Cr_{9.5}Al_{16}$ and β-Cr_5Al_8 phases were found to evolve apart from some free Cr (Fig. 10b). Rietveld structural refinement of the XRD profile for the coarse grade sample treated at 850 °C revealed about 62 wt.% $Cr_{9.5}Al_{16}$, 29 wt.% Cr_7Al_{45}, 4 wt.% β-Cr_5Al_8 and 3.5 wt.% of free Cr apart from very small fraction of Cr_2Al. Since all of Cr and Al in the blend remained in free-state even at 600 °C, it may be assumed that the phase formation at higher temperature (above 600 °C) possibly involves liquid phase due to melting of Al (m.p. of Al = 660 °C). The presence of the high temperature β-Cr_5Al_8 phase at lower temperature of 850 °C, which is otherwise expected only above ~1150 °C, possibly indicate that the peritectic reaction involving liquid Al initiates on the surface of the Cr particles, which leads to the formation of some amount of peritectic β-Cr_5Al_8. Under energetically favorable condition at 850 °C, a polymorphic transition leads to the ordered rhombohedral (*R3m*) $Cr_{9.5}Al_{16}$ structure. The formation of Al-rich Cr_7Al_{45} phase (monoclinic; space group: *C2/m*) possibly takes place by the diffusion of Cr in Al after melting of Al. It may be noted that Cr_2Al, Cr_7Al_{45} and the disordered β-Cr_5Al_8 phases were not observed at 850 °C in case of nanocrystalline powder precursors. The other interesting aspect of the results is the absence of any carbide phase in case of the powder blended by low-energy blender (Fig. 10). Carbon analysis of the coarse grade powder blends revealed no trace of carbon. The above observation indicates that the Cr_2AlC phase obtained during MA2 of the nanocrystalline precursor evolves preferentially from Cr_2Al, while the carburization of disordered β-Cr_5Al_8 and ordered $Cr_{9.5}Al_{16}$ phases are not favored in the temperature range of 400–850 °C.

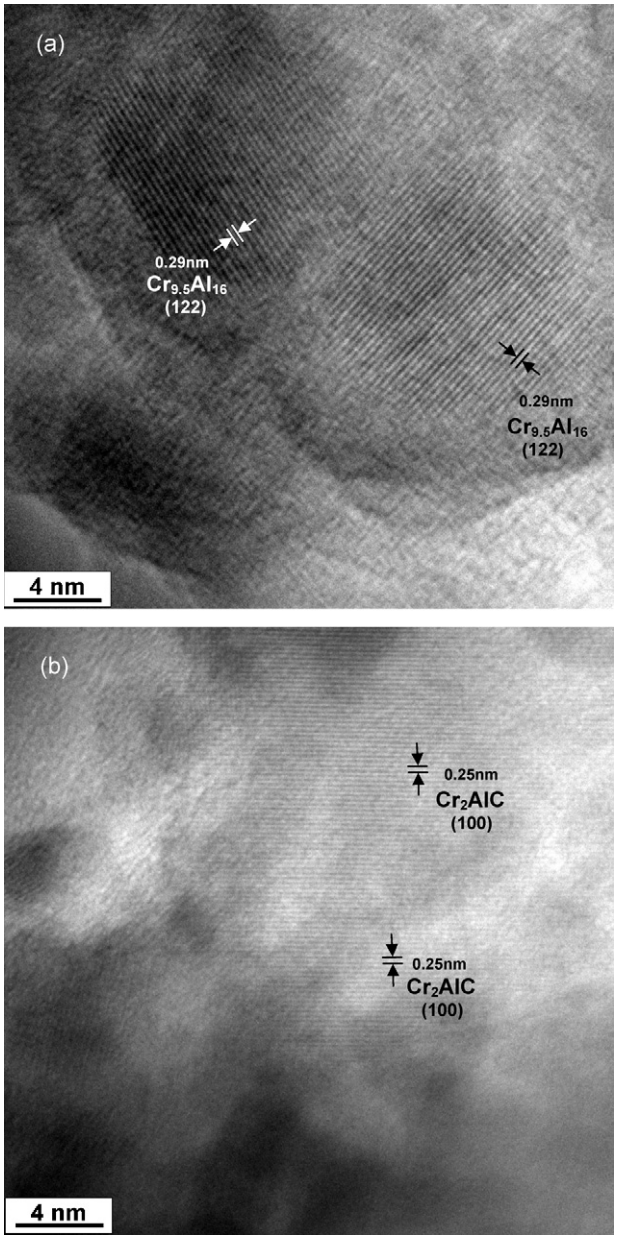

Fig. 8. TEM micrograph showing (a) (122) interplanar spacing of $Cr_{9.5}Al_{16}$ and (b) (1 0 0) interplanar spacing of Cr_2AlC in MA2 sample at 850 °C.

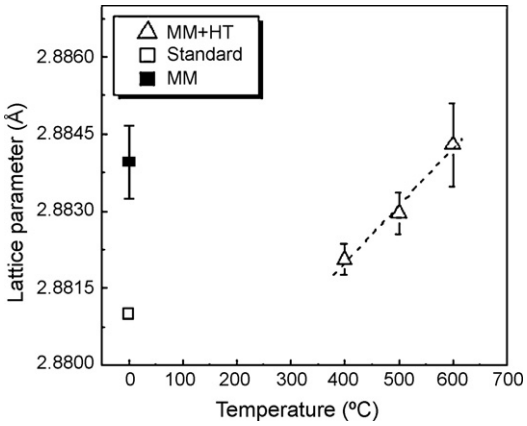

Fig. 9. Variation in the lattice parameter of Cr after milling and subsequent annealing.

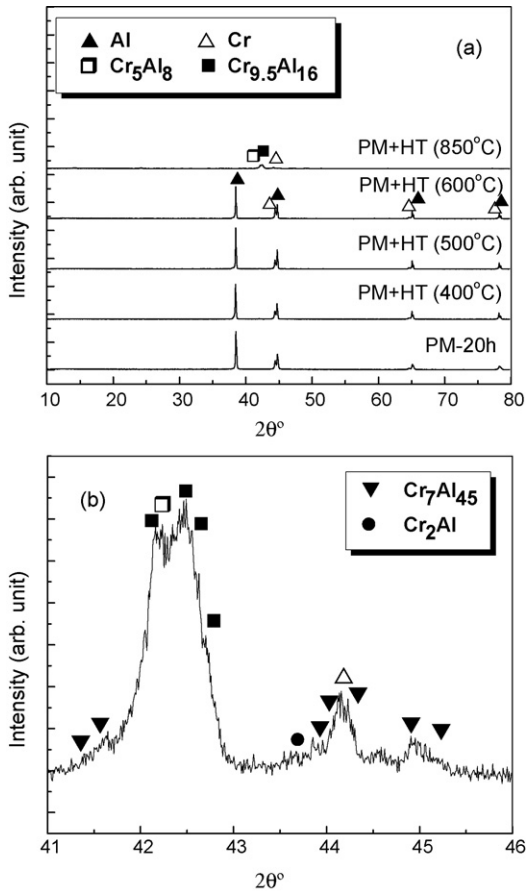

Fig. 10. (a) XRD profiles of the pot milled (PM) and subsequently heat treated (HT) samples at 400, 500, 600 and 850 °C. (b) Magnified section of the profile for PM + HT 850 °C.

4. Conclusions

Mechanically activated annealing of nanocrystalline Cr–60at.%Al powder blend led to the formation of various Cr–Al phases like Cr_2Al, $Cr_{9.5}Al_{16}$ and β-Cr_5Al_8 at a low temperature of 400 °C. Such diffusion-induced phase formation was observed only at a higher temperature of 850 °C in case of conventional coarse Cr–Al precursor with identical composition. The formation of Cr_2AlC phase was also observed in case of ball-milled nanocrystalline precursor, which contained about 2.65–2.80 wt.% of milling-induced C-contamination. The Cr_2AlC phase evolved on preferential carburization of Cr_2Al between 400 and 850 °C.

Acknowledgement

The authors acknowledge sincere help from Mr. K. Ramesh Reddy (ARCI) for experimental work.

References

[1] N. Malhouroux-Gaffet, E. Gaffet, J. Alloys Compd. 198 (1993) 143–154.
[2] L.L. Shaw, Mater. Manuf. Process. 15 (2001) 405–418.
[3] G.H. Chen, J. Alloys Compd. 416 (2006) 279–283.
[4] F. Neves, I. Martins, J.B. Correia, M. Oliveira, E. Gaffet, Intermetallics 16 (2008) 889–895.
[5] E. Barraud, S. Begin-Colin, G. Le Caer, O. Barres, F. Villieras, Int. J. Nanotechnol. 5 (2008) 649–659.
[6] Y.X. Chen, J.T. Li, J.S. Du, Mater. Res. Bull. 43 (2008) 1598–1606.
[7] M. Zakeri, M.R. Rahimipour, A. Khanmohammadian, Mater. Sci. Eng. A 492 (2008) 311–316.
[8] I.C.A. Adrian, G.A.O. Villalba, F.A. Deorsola, B. Benedetti, J. Alloys Compd. 466 (2008) 205–207.

[9] D. Maurya, H. Thota, K.S. Nalwa, A. Garg, J. Alloys Compd. 477 (2009) 780–784.
[10] S. Singh, M.M. Godkhindi, R.V. Krishnarao, B.S. Murty, J. Eur. Ceram. Soc. 29 (2009) 2069–2077.
[11] D.P. Xiang, Y. Liu, M.J. Tu, Y.Y. Li, W.P. Chen, Int. J. Refract. Met. Hard Mater. 27 (2009) 111–114.
[12] M.N. Samani, A.R. Kamali, R. Mobarra, M.N. Samani, Mater. Lett. 64 (2010) 309–312.
[13] V. Udhayabanu, K.R. Ravi, V. Vinod, B.S. Murty, Intermetallics 18 (2010) 353–358.
[14] R. Yazdani-rad, S.A. Mirvakili, M. Zakeri, J. Alloys Compd. 489 (2010) 379–383.
[15] H.W. Kerr, J. Cisse, G.F. Bolling, Acta Metall. 22 (1974) 677–686.
[16] J.S. Kim, Y.S. Kwon, G.V. Golubkova, O.I. Lomovsky, D.Y. Dudina, L.S. Davlitova, V.V. Malakhov, S.F. Tikhov, V.V. Usol'tsev, V.A. Sadykov, Inorg. Mater. 44 (2008) 587–591.
[17] V.I. Fadeeva, A.V. Leonov, E. Szewczak, H. Matyja, Mater. Sci. Eng. A 242 (1998) 230–234.
[18] N. Forouzanmehr, F. Karimzadeh, M.H. Enayati, J. Alloys Compd. 471 (2009) 93–97.
[19] F. Zhang, L. Lu, M.O. Lai, J. Alloys Compd. 297 (2000) 211–218.
[20] F.G. Cuevas, J.M. Montes, J. Cintas, J.M. Gallardo, Powder Metall. 48 (2005) 365–370.
[21] M.R. Farhang, A.R. Kamali, M.N. Samani, Mater. Sci. Eng. B 168 (2010) 136–141.
[22] C.C. Koch, J.S.C. Jang, P.Y. Lee, in: E. Arzt, L. Schultz (Eds.), New Materials by Mechanical Alloying, DGM Confer. Calw-Hirsau, DGM Informationsgesellschaft Verlag, 1988, pp. 101–110.
[23] L. Lu, M.O. Mai, S. Zhang, J. Mater. Process Tech. 48 (1995) 683–690.
[24] A. Mashreghi, M.M. Moshksar, J. Alloys Compd. 484 (2009) 957–960.
[25] E. Ivanov, T. Grigorieva, G. Golubkova, V. Boldyrev, A.B. Fasman, S.D. Mikhailenko, O.T. Kalinina, Mater. Lett. 7 (1988) 51–54.
[26] O.C. Alonso, J.G.C. Moreno, J.J.C. Rivera, G.F. Diaz, A. Ita, S.Q. Molina, C. Falcony, Mater. Sci. Forum. 343 (2000) 290–295.
[27] Á. Csanady, A.C. Pintér, L. Varga, L. Tóth, G. Vincze, J. Phys. I 6 (1996) 925–940.
[28] S.K. Pabi, J. Joardar, I. Manna, B.S. Murty, NanoStruct. Mater. 9 (1997) 149–152.
[29] S. Shinya, I. Tsuyoshi, U. Minoru, O. Isao, J. Jpn. Soc. Powder. Powder. Metall. 38 (1991) 971–975.
[30] M. Zdujic, D. Poleti, Lj. Karanovic, K.F. Kobayashi, P.H. Shingu, Mater. Sci. Eng. A 185 (1994) 77–86.
[31] S. Enzo, G. Mulas, F. Delogu, R. Frattini, Mater. Sci. Forum 312–314 (1999) 417–422.
[32] F.A. Santos, A.S. Ramos, C. Santos, D. Rodrigues, J. Alloys Compd. 491 (2010) 187–191.
[33] F. Bai, Z. Chai, K. Qi, T. Li, L. Lu, J. Alloys Compd. 486 (2009) 801–804.
[34] J.G. Costa Neto, C.A. Sergio Gama, Ribeiro, J. Alloys Compd. 182 (1992) 271–280.
[35] M. Audier, M. Durand-Charre, E. Laclau, H. Klein, J. Alloys Compd. 220 (1995) 225–230.
[36] B. Grushko, E. Kowalska-Strzjeciwilk, B. Przepiïorzyïnski, M. Surowiec, J. Alloys Compd. 402 (2005) 98–104.
[37] Y. Liang, C. Guo, C. Li, Z. Du, J. Alloys Compd. 460 (2008) 314–319.
[38] J.L. Murray, in: T.B. Massalski (Ed.), Binary Alloy Phase Diagrams, 2nd ed., ASM International, Metals Park, OH, 1990, pp. 138–140.
[39] K. Naplocha, K. Granat, J. Alloys Compd. 480 (2009) 369–375.
[40] D. Vojtˇech, J. Verner, J. ˇSerïak, F. ˇSimanˇcïık, M. Balog, J. Nagy, Mater. Sci. Eng. A 458 (2007) 371–380.
[41] P.J. Ozawa, S. Yoshizaki, S. Takeyama, T. Enjo, K. Ikeuchi, IEEE Transactions. CHMT-9 4 (1986) 391–395.
[42] J. Rodriguez-Carvajal, Program FullProf.2k, Version 4.00, LLB-CEA-CNRS, France, 2007.
[43] B.D. Cullity, Elements of X-ray diffraction, 2nd ed., Addison-Wesley, Reading, MA, USA, 1978.
[44] W.B. Tian, P.L. Wang, Y.M. Kan, G.J. Zhang, Y.X. Li, D.S. Yan, Mater. Sci. Eng. A 443 (2007) 229–234.
[45] Z.J. Lin, Y.C. Zhou, M.S. Li, J.Y. Wang, Z. Metall. 96 (2005) 291–296.
[46] W. Tian, P. Wang, G. Zhang, Y. Kan, Y. Li, D. Yan, Scr. Mater. 54 (2006) 841–846.
[47] J.J. Poubeau, J. Bigot, Acta Metall. 33 (1985) 1137–1141.
[48] J.A. Dean, Lange's Handbook of Chemistry, 15th ed., McGraw-Hill, 1999.